Oriented Thin Films of a Benzodithiophene Covalent Organic Framework

Dana D. Medina,[†] Veronika Werner,[†] Florian Auras,[†] Raphael Tautz,[‡] Mirjam Dogru,[†] Jörg Schuster,[†] Stephanie Linke,[†] Markus Döblinger,[†] Jochen Feldmann,[‡] Paul Knochel,[†,*] and Thomas Bein[†,*]

[†]Department of Chemistry and Center for NanoScience (CeNS), University of Munich (LMU), Butenandtstrasse 5-13, Haus E, 81377 München, Germany, and [‡]Photonics and Optoelectronics Group, Department of Physics and Center for NanoScience (CeNS), University of Munich (LMU), Amalienstrasse 54, 80799 München, Germany

ABSTRACT A mesoporous electron-donor covalent organic framework based on a benzodithiophene core, BDT-COF, was obtained through condensation of a benzodithiophene-containing diboronic acid and hexahydroxytriphenylene (HHTP). BDT-COF is a highly porous, crystalline, and thermally stable material, which can be handled in air. Highly porous, crystalline oriented thin BDT-COF films were synthesized from solution on different polycrystalline surfaces, indicating the generality of the synthetic strategy. The favorable orientation, crystallinity, porosity, and the growth mode of the thin BDT-COF films were studied by means of X-ray diffraction (XRD), 2D grazing incidence diffraction (GID), transmission and scanning electron microscopy (TEM, SEM), and krypton sorption. The highly porous thin BDT-COF films were infiltrated with soluble fullerene derivatives, such as [6,6]-phenyl C_{61} butyric acid methyl ester (PCBM), to obtain an interpenetrated electron-donor/acceptor host–guest system. Light-induced charge transfer from the BDT-framework to PCBM acceptor molecules was indicated by efficient photoluminescence quenching. Moreover, we monitored the dynamics of photogenerated hole-polarons *via* transient absorption spectroscopy. This work represents a combined study of the structural and optical properties of highly oriented mesoporous thin COF films serving as host for the generation of periodic interpenetrated electron-donor and electron-acceptor systems.

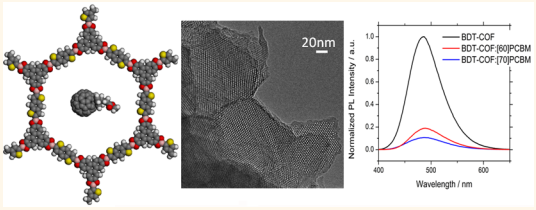

KEYWORDS: covalent organic frameworks (COFs) · porous materials · thin films · interpenetrated systems

Covalent organic frameworks (COFs) are promising materials for host–guest studies due to their high specific surface area, defined pore size, crystalline structure, and great structural diversity.[1−7] So far, COFs have mainly been studied as potential host materials for gas storage and catalysis applications.[8−11] However, COFs have recently been proposed as interesting candidates for applications in organic electronics due to the successful incorporation of photoactive building blocks into the frameworks.[12−21] The latter interest is based on their beneficial stacking behavior, which allows one to create structures with a significant degree of order. 'Two-dimensional' COFs are synthesized from planar building blocks to give extended sheet-like structures. These two-dimensional structures assemble into crystalline three-dimensional materials *via* dispersive forces (π-stacking). The π-stacked layers in these COFs are thought to offer a pathway for charge transport.[22,23] Furthermore, the porous nature of the COFs allows for the infiltration of suitable complementary photoactive/semiconducting guest species.[18,19] Thus, charge separation in highly ordered donor–acceptor interpenetrated architectures can be studied.[18] To implement COF structures in photovoltaic devices and to study the charge separation in interpenetrated architectures, the fabrication of highly oriented thin COF films is essential.[24−28] Great efforts have been invested in developing new deposition methods of photoactive polymers and photoactive polymer blends as ordered thin films in order to study the charge transport in the ordered domains.[29] The growth of highly crystalline oriented thin COF films can provide an access to a suitable architecture for charge migration toward the respective electrodes. Furthermore, oriented COF thin films can provide open straight

* Address correspondence to tbein@cup.uni-muenchen.de, paul.knochel@cup.uni-muenchen.de.

Received for review January 2, 2014 and accepted February 23, 2014.

Published online February 24, 2014
10.1021/nn5000223

channels that facilitate the infiltration of the acceptor units into the framework pores. Very recently, Jiang *et al.* introduced the conjugated and stable COF (CS-COF), which showed photovoltaic conversion efficiency of up to 0.9% when mixed, as a powder, with electron acceptor units and spincoated on an electrode. In that report, the authors emphasized the need to control the COF growth on the desired substrate to obtain better performance.[30]

Regardless of the potential of COFs for photovoltaic applications, their highly ordered organic channels position COFs as interesting nanoscale template materials. In previous work, highly ordered inorganic mesoporous materials have been used as templates for the growth of a large variety of compounds such as carbon nanowires and mesoporous polymers.[31−33] However, it has been a long-standing challenge to achieve vertical orientation of ordered nanochannel systems on a substrate.[34−38] In this context, the "organic" pores of COFs are intriguing candidates for oriented growth on various substrates. Such systems would provide vertical, crystalline nanochannels offering a great scope for molecular functionalization and associated functionality. Dichtel *et al.* introduced the first oriented thin COF films on substrate-supported single layer graphene (SLG), since these provide a suitable substrate for the COF growth through favorable π-interactions with the surface.[39] Later, COFs with greater pore sizes based on large chromophores were synthesized as oriented thin films on substrate-supported SLG.[40]

Herein, we describe the synthesis of a new COF structure based on benzo[1,2-b:4,5-b′]dithiophene-2,6-diyldiboronic acid, serving as an electron donor building block in a covalent organic framework. We introduce, for the first time, oriented thin benzodithiophene COF (BDT-COF) films on indium-doped tin oxide (ITO) substrates with and without a hole-selective blocking layer, such as NiO. Furthermore, the growth of thin BDT-COF films was studied on gold surfaces to illustrate the generality of the synthesis method. Finally, oriented BDT-COF films were grown on fused silica substrates in order to study the optical properties of these highly oriented BDT-COF films. The BDT core has attracted significant interest as a component of organic photoactive polymers.[41−44] BDT shows excellent light absorption properties when co-polymerized with thienothiophene groups or in donor−acceptor polymers.[43,45,46] It is therefore of great interest to implement a BDT core into a well-ordered crystalline porous material, such as a COF, and to study its physical and optical properties in the form of oriented thin films.

RESULTS AND DISCUSSION

BDT-COF Bulk Characterization. The new thiophene based COF, BDT-COF, was synthesized under solvothermal conditions by the co-condensation of benzo[1,2-*b*:4,5-*b*′]dithiophene-2,6-diyldiboronic acid (BDTBA) and the polyol 2,3,6,7,10,11-hexahydroxytriphenylene (HHTP; Figure 1a). A detailed description of the reaction parameters is given in the Methods section.

Powder X-ray diffraction (PXRD) clearly indicates the formation of a highly crystalline COF. Its *d*-values are in agreement with a hexagonal unit cell with $a = b = 36.9$ Å as expected from the planar co-condensation reaction presented in Figure 1a. For previous COF structures different packing arrangements of the hexagonal planar sheets were reported. Thus, to determine the packing arrangement of the new crystal, structure simulations were carried out. Two possible crystal packing modes, namely, eclipsed AA and staggered AB, together with their corresponding PXRD patterns were simulated with Materials Studio software (see Figures S1−S4 in the Supporting Information). For the simulations of the eclipsed AA arrangement, we chose the idealized packing of the *P6/m* space group where the π-electrons are fully overlapped. However, we note that other AA packing arrangements are possible (see Figures S5−S8 in the Supporting Information). The simulated powder pattern was then compared to the experimentally obtained pattern. The experimental PXRD pattern for BDT-COF agrees very well with the simulated pattern and confirms the formation of an eclipsed AA arrangement (Figure 1b). The unit-cell parameters, determined from the experimental X-ray patterns, match very well with those obtained from the structure simulations.

The presence of the boronate ester functionality was verified with FT-IR spectroscopy. The most characteristic modes of the asymmetric B−O and C−O functionalities can be assigned to the bands at 1347 and 1240 cm^{-1} (Figure S9, Supporting Information). The ^{11}B MAS NMR spectrum (Figure S10, Supporting Information) shows a trigonal-planar boron atom with a chemical shift of δ = 19.98 ppm, which can be distinguished from that in the starting material (BDTBA: δ =15 ppm).

The porosity of BDT-COF was characterized by nitrogen sorption measurements at 77.3 K. A mesoporous structure was confirmed by the characteristic type IV isotherm (Figure 2a), which shows a strong rise in the nitrogen uptake at relatively low partial pressure as a result of the highly defined mesoporous system. The Brunauer−Emmett−Teller (BET) surface area was calculated ($P/P_0 = 0.09−0.18$ in the adsorption branch) to be as high as 1946 $m^2\ g^{-1}$, and the pore volume to be 1.39 $cm^3\ g^{-1}$. The isotherm evaluation, carried out with an NLDFT-based kernel, yields a pore size of 3.4 nm (Figure 2b). The theoretical values for the surface area and pore volume of BDT-COF with an eclipsed structure were calculated with the Connolly surface area method to be 2051 $m^2\ g^{-1}$ and 1.43 $cm^3\ g^{-1}$,

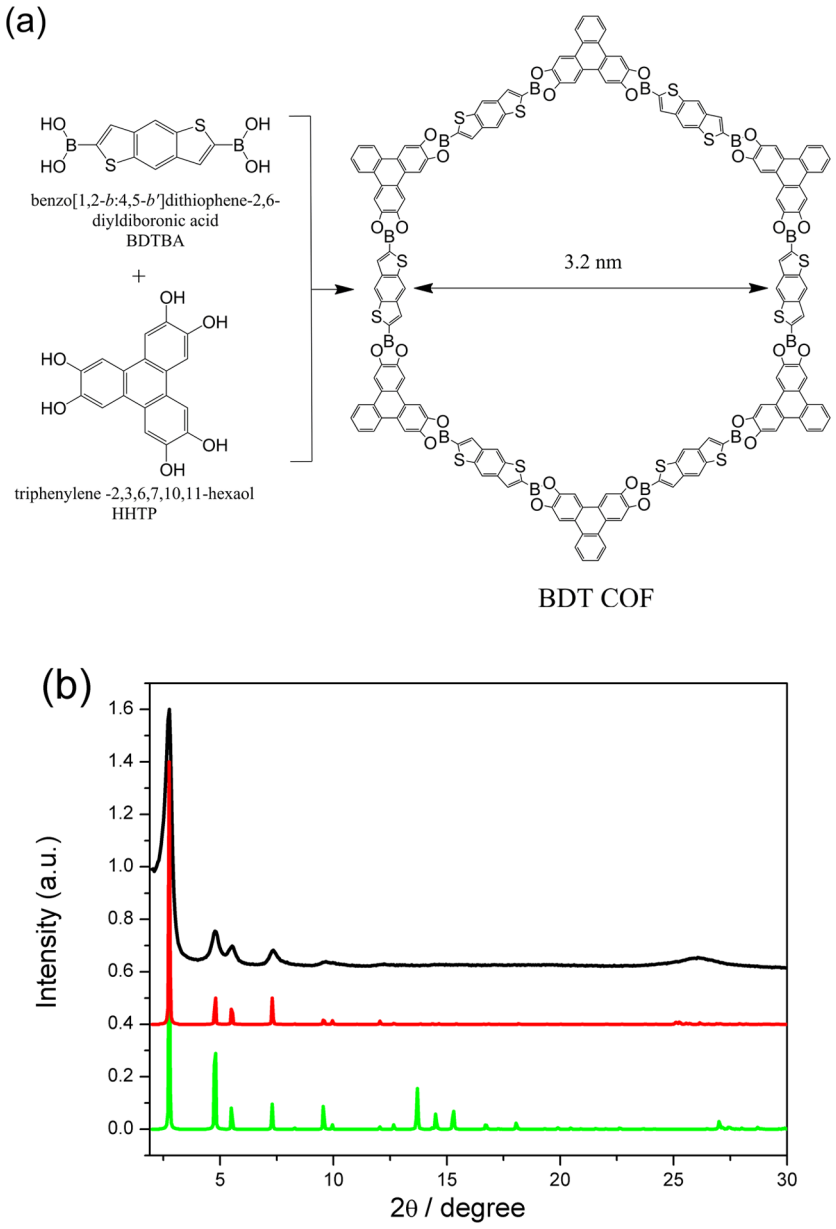

Figure 1. (a) Reaction scheme for the co-condensation of BDT-COF. (b) Experimentally obtained PXRD pattern (black), simulated patterns obtained by the Reflex module in MS Studio, based on an eclipsed AA arrangement in (red) and a staggered AB arrangement in (green).

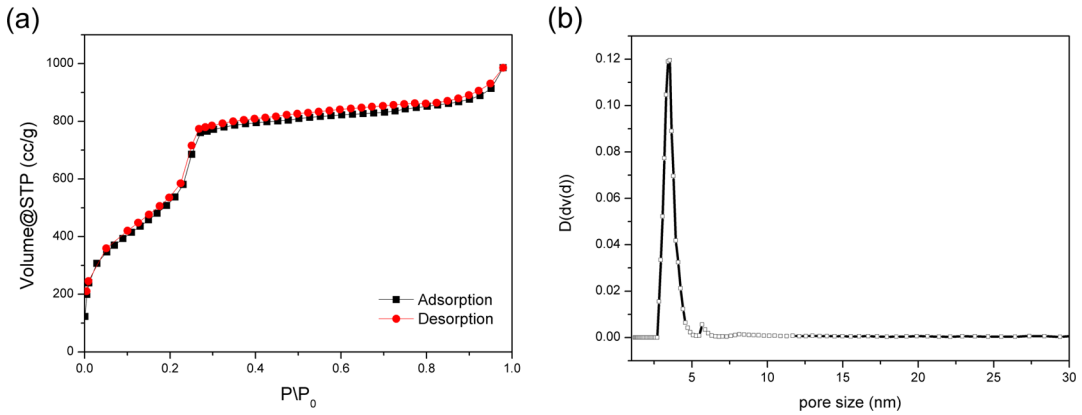

Figure 2. (a) Nitrogen sorption isotherm of degassed BDT-COF measured at 77.3 K. (b) Pore size distribution of degassed BDT-COF.

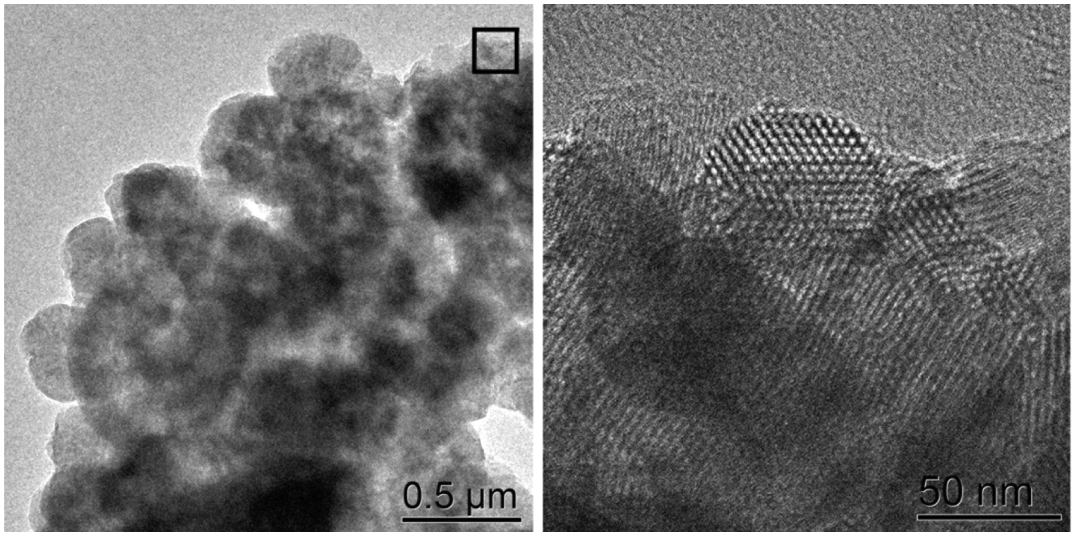

Figure 3. TEM micrographs of bulk polycrystalline BDT-COF showing cauliflower morphology at low magnification (left). The black square indicates the magnified detail area on the right, showing randomly oriented crystalline BDT-COF with domain sizes of about 50 −100 nm.

respectively. This is in good agreement with the experimental surface area and experimental pore volume obtained from the sorption data.

Thermogravimetric analysis showed that a major mass loss takes place at 400 ° C. We attribute this mass loss to the decomposition of BDT-COF (Figure S12, Supporting Information). The BDT-COF bulk material absorbs strongly at wavelengths below 430 nm (Figure S13 Supporting Information).

Scanning electron microscopy (SEM) of bulk BDT-COF showed small crystals with sizes of about 50 nm. These crystals tend to aggregate into larger domains (Figure S15, Supporting Information). Transmission electron microscopy (TEM) analysis revealed an intergrown cauliflower morphology of the polycrystalline BDT-COF, where the top view along the *c*-axis showed hexagonal structures with a pore size of about 3.3 nm. In addition, pores with distinct sizes and long ordered channels were observed in a tilted view of the crystallites (see Figure 3).

The bulk characterization confirms the formation of a new highly crystalline COF structure based on BDT building blocks. This structure is highly porous and exhibits a well-defined pore size. As already mentioned, in order to study the optical/optoelectronic properties of COF nanostructures or to utilize these structures as highly defined template materials, it is desirable to develop methods for the deposition of thin COF films on suitable surfaces.

BDT-COF Thin films. Transparent substrates coated with conductive and transparent layers, such as indium-doped tin oxide, are of greatest importance for fabricating photovoltaic devices.[47] Therefore, we present a new approach for the synthesis of BDT-COF on different metal oxide substrates. Thin BDT-COF films were synthesized under similar solvothermal conditions as described for the case of bulk BDT-COF, but with a lower concentration of starting materials in the solvent mixture. In addition, ITO-coated glass substrates were immersed face downward into the reaction mixture with the aid of a Teflon holder (for more details, see Methods). Top-view SEM analysis of the obtained films revealed a smooth and homogeneous coverage of organic material on the surface of the ITO-coated glass substrate (Figure S16, Supporting Information). Cross-sectional SEM analysis clearly shows the formation of the organic dense thin film on the ITO thin layer with a uniform thickness of about 150 nm. The thin organic film appears crack-free and with a good adherence to the ITO surface, forming a high-quality ITO−COF interface. (Figure 4a).

To study the degree of crystallinity of the obtained thin films, a detector scan X-ray diffraction analysis was performed. The detector scan measurements revealed the disappearance of all reflections assigned to the mesoporous structure at low 2θ angles. The strong and sharp reflection at 26.1° 2θ is related to the π-stacking of the 2D COF layers (Figure 4b). All other reflections at high angles are attributed to the ITO film. This result suggests a preferential orientation of the COF structure within the thin film on the ITO surface, implying that the COF layers are aligned parallel to the substrate surface. Effective domain sizes of 11 $\pm$ 3 nm in *c*-direction of BDT-COF were calculated using the Scherrer equation for peak broadening.[48] To further examine the preferred orientation, grazing incidence diffraction (GID) investigations were carried out by grazing incidence small and wide-angle X-ray scattering analysis (GI-SWAXS), which provides 2D information on structure and orientation. The reflections observed can be indexed according to the BDT-COF structure observed in the bulk (Figure 4c). We calculated the lattice

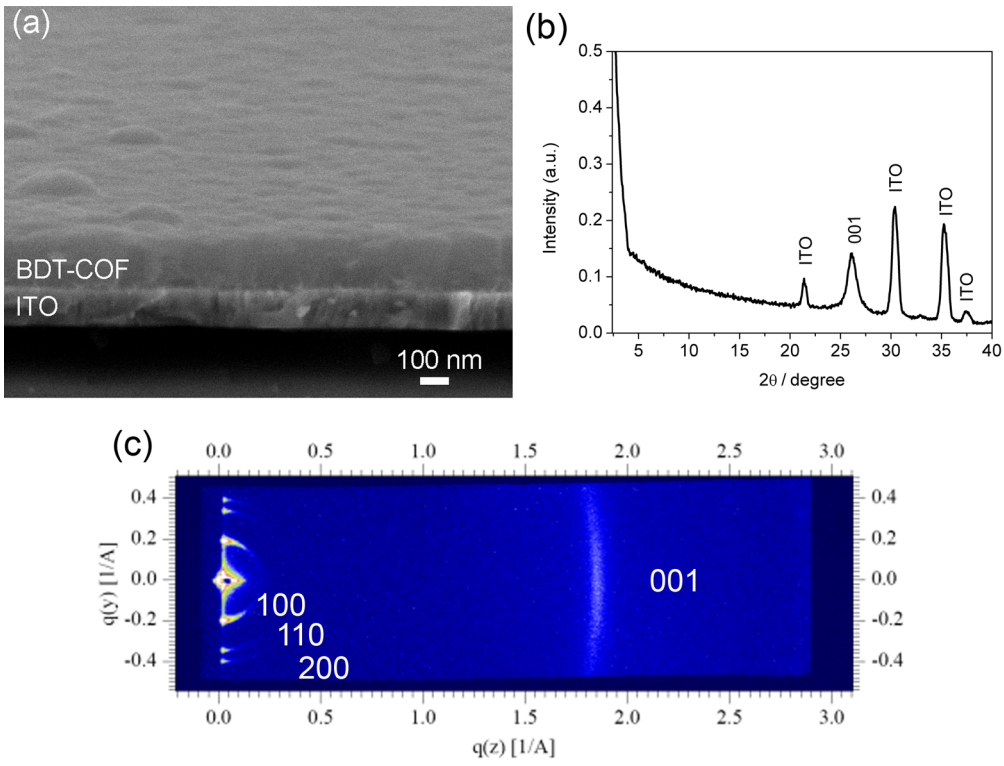

Figure 4. (a) SEM micrograph (cross section) of BDT-COF thin film grown on an ITO-coated glass substrate. (b) X-ray diffraction pattern (detector scan geometry) taken for BDT-COF thin film grown on ITO-coated glass. (c) 2D-GID analysis for BDT-COF thin film grown on ITO-coated glass.

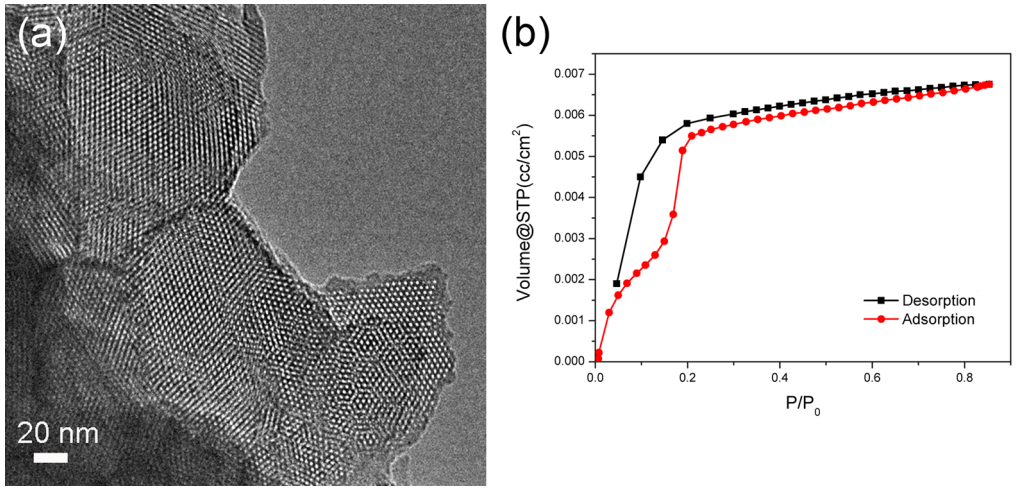

Figure 5. (a) TEM micrograph of BDT-COF thin film fragment showing the hexagonal structure along the *c*-axis. (b) Krypton sorption isotherm of degassed BDT-COF thin film on ITO-coated glass measured at 77.3 K.

parameter for a hexagonal structure, $a = b = 36.9$ Å; this value is in a very good agreement with the calculated values for the simulated and the bulk BDT-COF structure. The reflections (in Figure 4c) centered near $q(z) = 0$ indicate that indeed preferential orientation of the COF layers was obtained, with the [001]-axis (*c*-axis) oriented orthogonal to the surface, and rotational freedom around this axis. This is consistent with previous reports of COF structures grown on SLG.[39] The 001 reflection is observed as a diffuse arc of scattering at $q(z) = 1.85$ Å^{-1}, which indicates a moderate angular spread of the stacking direction and confirms that the *c*-axis is orthogonal to the substrate surface. A crystal domain size of about 25 nm within the *ab*-plane was determined from the scattering data. TEM samples of the same film were prepared by removing the BDT-COF film with a fine blade from the ITO surface and then transferring it onto a copper grid supporting a thin, electron transparent carbon film. Thus, projections along the film normal were observed in the TEM (Figure 5a). In

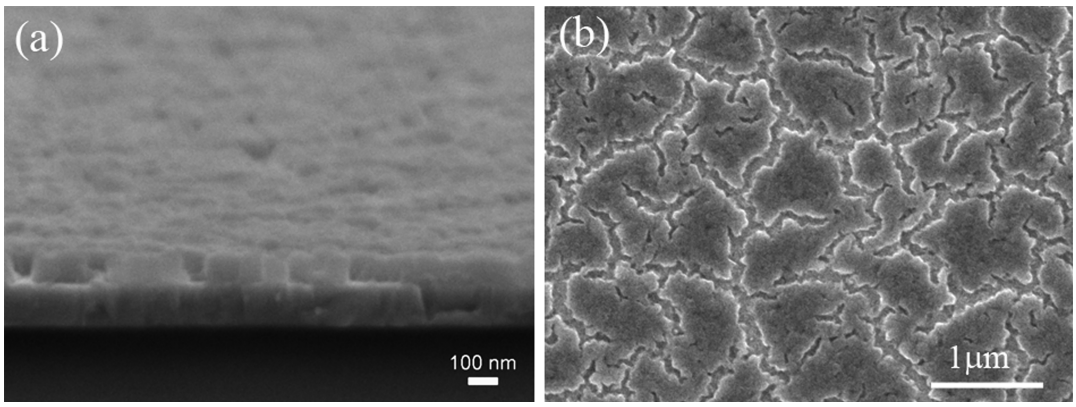

Figure 6. SEM micrograph in cross section (a) and in top view (b) of BDT-COF thin film grown on an ITO-coated glass substrate, within short reaction time.

agreement with the GID measurements, almost exclusively hexagonal structures were observed with the pore channels orthogonal to the surface. Electron diffraction patterns taken from a large number of BDT-COF crystallites confirm this observation (Figure S14, Supporting Information).

To make thin porous film systems accessible for guest molecules, the framework should not only be well aligned, but must also be free of starting materials and undesired solvent residues. The porosity must be maintained throughout the synthesis and subsequent treatments. For an assessment of the porosity of thin BDT-COF films, krypton sorption was employed. Krypton sorption measurements at 77.3 K showed the characteristic type IV isotherm for mesoporous structures (Figure 5b).[49] The adsorption branch confirmed the narrow pore size distribution by the sharp rise in the krypton uptake at relatively low partial pressures. The BET surface area was calculated to be as high as 175 cm^2/cm^2 (P/P_0 = 0.03−0.1 of the adsorption branch). The characterization of the above thin film samples demonstrates the formation of a porous crystalline thin BDT-COF film on a transparent conductive substrate with homogeneous thickness and coverage. Furthermore, it proves the presence of a highly oriented film with a preferential orientation in *c*-direction. This architecture also favors the infiltration of potential guest molecules. However, if an interpenetrated system is desired, implying that complementary donor/acceptor molecules fill the COF pores, an appropriate charge carrier-selective layer must be implemented. We therefore incorporated a nickel oxide layer on the ITO surface as a model system for inorganic metal oxide blocking layers. The NiO layer was synthesized using a solution-processing route with nickel acetate tetrahydrate ($Ni(OAc)_2 \cdot 4H_2O$) in the presence of monoethanolamine in ethanolic solution.[50] The green NiO precursor solution was spin-coated on the ITO coated-glass substrate. The latter was then heated to 300 °C on a hot plate to form a uniform NiO layer of 10 nm thickness (Figure S17, Supporting Information). In the next step, BDT-COF was synthesized as a thin film as described above. At the end of the solvothemal synthesis, a high-quality thin COF film was obtained on the surface of the NiO/ITO-coated glass. SEM analysis revealed an organic thin film with a thickness of 150 nm that adhered very well to the NiO layer (Figure S17, Supporting Information). Consistent with the X-ray data of the BDT-COF on the plain ITO-coated glass surface (Figure 4b, c), the thin BDT-COF film is oriented with the *c*-axis parallel to the surface normal (Figure S18a, Supporting Information). TEM analysis of removed fragments of the thin BDT-COF film also confirmed the preferential orientation along the c-direction (Figure S18b, Supporting Information). Similarly, krypton sorption revealed a type IV isotherm, corresponding to the mesoporous structure with a narrow pore size distribution indicated by the steep rise of the adsorption branch at about P/P_0 = 0.2. The BET surface area for this film was calculated as 145 cm^2/cm^2 (P/P_0 = 0.03−0.1 of the adsorption branch, Figure S18c, Supporting Information).

The newly discovered growth of oriented thin COF films on different polycrystalline inorganic substrates shows that favorable π-interactions of the monomers or COF oligomers with the surface play a minor role in achieving preferential orientation. To shed light on the growth process of BDT-COF, we examined the COF film morphology at the first steps of formation. The synthesis of thin BDT-COF films on ITO coated-glass was performed at similar conditions as described above and interrupted after 2 h. SEM cross section analysis revealed a thin film of approximately 70 nm thickness composed of free-standing pillars in close vicinity (see Figure 6). Consistent with the thin BDT-COF film on ITO coated-glass, the X-ray diffraction pattern (Figure S19, Supporting Information) indicates the formation of a thin COF film with a preferential orientation along the c-direction. The broadening of the 26.1° reflection indicates that crystal domains in the *c*-direction are smaller than after longer reaction times. We note that the oriented thin BDT-COF film grows through an

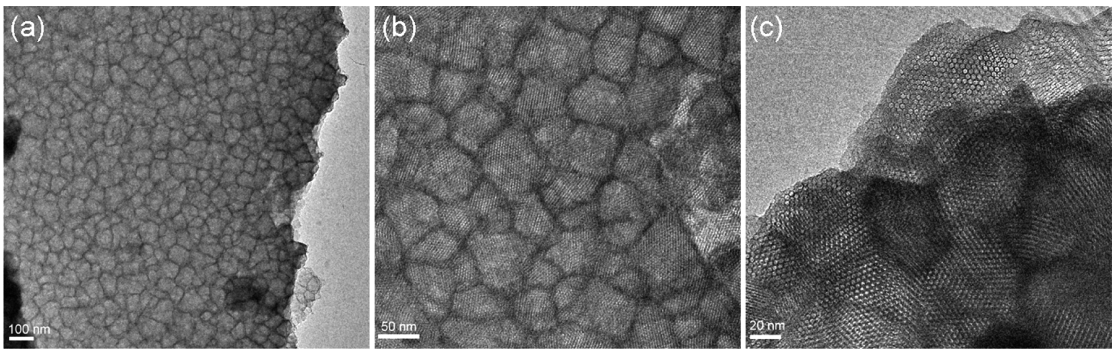

Figure 7. TEM micrographs of BDT-COF thin film fragment grown on a gold surface showing the hexagonal structure along the *c*-axis at different magnifications.

island formation mechanism. Apparently, the growth of BDT-COF film in the *c*-direction is fast, while the lateral growth occurs at slower rates.

To study the impact of the nature of the surface on film growth, we investigated the growth of BDT-COF as thin film on additional substrates. For example, gold substrates were prepared by sputtering methods.[51] The synthesis of BDT-COF was carried out under the same reaction conditions as for the growth on metal oxide surfaces, where a freshly prepared gold substrate replaced the ITO-coated glass. GID investigations confirmed the formation of oriented thin films along the *c*-axis, consistent with the GID experiments of thin BDT-COF film grown on ITO (Figure S20, Supporting Information). TEM analysis revealed a highly oriented thin COF film along the *c*-axis. The film consists of small COF crystallites with distinct grain boundaries complementary in shape, thus achieving a long-range dense coverage. (Figure 7 a-c).

Thin COF films grown on appropriate substrates allow for investigating their optical/optoelectronic properties. Charge transfer from a COF to acceptor species in its pore system has been reported for thienothiophene-based COFs.[18,19] We have demonstrated that the infiltration of [6,6]-phenyl C_{61} butyric acid methyl ester ([60]PCBM) into a thienothiophene-containing COF (TT-COF) powder led to a complete quenching of the COF photoluminescence, indicating electron injection from the COF donor to the PCBM acceptor.[18] To study the electron transfer capabilities of the BDT-COF, photoluminescence (PL) quenching experiments with the fullerene derivatives [60]PCBM and [70]PCBM were preformed. Oriented COF films of 150 nm thickness were grown on fused silica serving as a nonquenching substrate and subsequently infiltrated with the respective electron acceptor *via* spin-coating of a 20 mg/mL solution in 1,2-dichlorobenzene. This procedure was found to result in good pore filling and additionally to create a thin PCBM overlayer.[18] The UV−vis spectra of the BDT-COF films before and after PCBM infiltration (Figure 8a) appear as a superposition of the absorbance spectra of the COF and of the respective fullerene. The absence of any observable change in the UV−vis spectrum of the BDT-COF upon fullerene infiltration indicates that no change in the electronic structure of the COF or degradation of the framework occurred. This was further confirmed by XRD measurements after infiltration (Figure S21, Supporting Information). Upon excitation at 365 nm, the pristine BDT-COF exhibits PL centered at 485 nm (Figure 8b). When infiltrated with electron acceptor molecules, this PL is considerably reduced in intensity. We note that the observed decrease in intensity (solid blue and green lines) is partially due to absorption of the emitted light by the fullerene phase. When correcting for this (dashed lines), infiltration with [60]PCBM or [70]PCBM causes a quenching of the COF PL of about 60% in both cases. Some of the remaining PL might be due to the possible existence of disordered domains in the film that are not accessible to the PCBM solution.

A further indication for charge separation is the formation of polarons in both the electron donor and electron acceptor constituents.[52−54] Upon illumination, excitons and bound polarons are expected to form on the COF backbone and dissociate into free polarons by electron transfer to closely located acceptor molecules at the donor−acceptor interface. Ultrafast femtosecond spectroscopic studies, exciting the BDT-COF close to its optical bandgap at 400 nm, and probing the polaron absorption at a suitable wavelength allows us to gain insights into the polaron decay dynamics. To study the formation of hole-polarons within the electron-donor constituent, *i.e.*, BDTBA assembled in an oriented BDT-COF film, first the respective absorption spectrum (cation absorption) was retrieved (Figure S22, Supporting Information) by chemical oxidation experiments and sequential absorption measurements (as detailed in the Supporting Information section 10). According to this study, a wavelength of 650 nm was found to be suitable for probing the hole-polarons in thin BDT-COF films, corresponding to the red tail of the polaron absorption. The chosen probe wavelength allowed us to isolate the polaron absorption from other spectral contributions, such as ground state absorption and stimulated

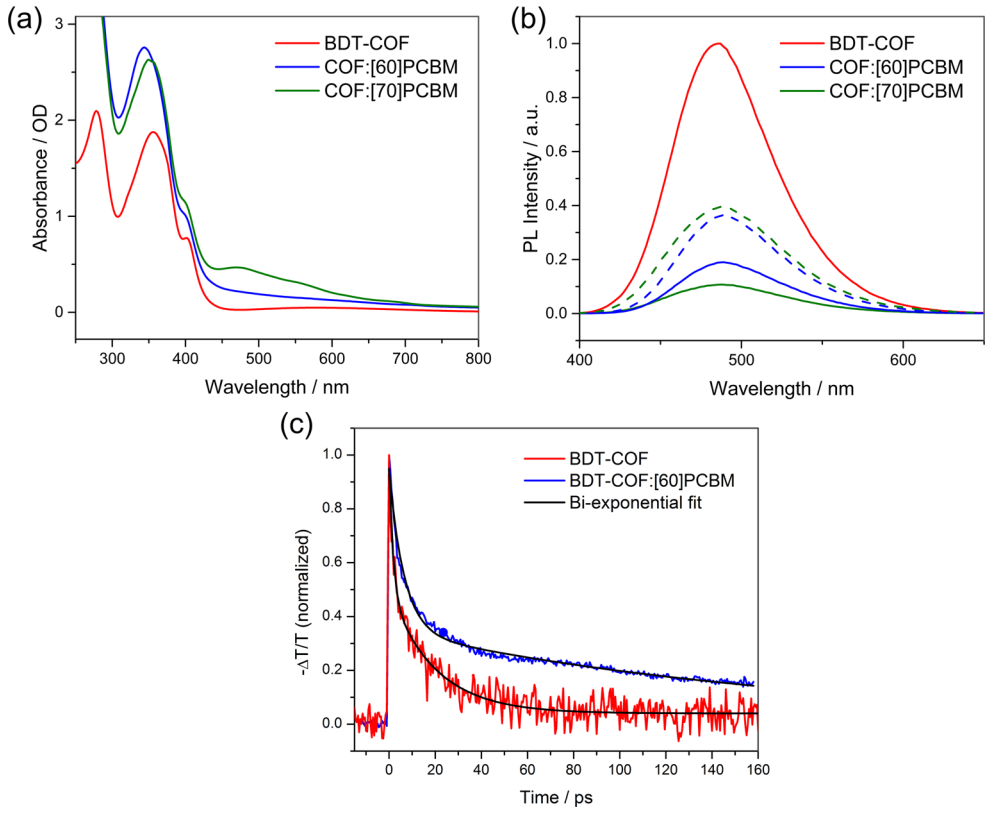

Figure 8. (a) Absorbance spectrum of films of BDT-COF grown on a quartz substrate (red), of BDT-COF:[60]PCBM (blue), and of BDT-COF:[70]PCBM (green), respectively. (b) Photoluminescence spectra of films of BDT-COF (red), BDT-COF:[60]PCBM (blue), and BDT-COF:[70]PCBM (green) obtained using an excitation wavelength of 365 nm. The dashed curves are the PL spectra after correction for absorption of emitted light by the PCBM. (c) Femtosecond pump−probe transient absorption measurements of BDT-COF (red), and BDT-COF:[60]PCBM (blue) hole-polaron lifetime, together with best-fitting biexponential curves (black). Pump wavelength was 400 nm; probe wavelength was 650 nm.

emission of excitons. The normalized transient-absorption signals of hole-polarons, together with the best fit biexponential decays curves, are shown in Figure 8c. The fitted curve of hole-polaran decay dynamics of the pristine thin BDT-COF film revealed two decay times, τ_1 = 1.7 ± 0.3 ps and τ_2 = 19.7 ± 1.5 ps. In the case of the BDT-COF:[60]PCBM interpenetrated system, we measured a significantly stronger signal than in the pristine COF film, which can be seen in a significantly improved signal-to-noise ratio, showing longer decay times, *i.e.*, τ_1 = 6.5 ± 0.2 ps and τ_2 = 178 ± 4 ps (attributed to geminate and nongeminate recombination, respectively). The stronger signal in combination with a longer liftetime clearly indicates charge dissociation and formation of polarons at the donor/acceptor interface. A further indication for efficient electron transfer from the COF to the [60]PCBM is provided by the very similar lifetime decay characteristics of electron-polarons in [60]PCBM (anion absorption probed at 1050 nm)[55] compared to the lifetime decay of hole-polarons (Figure S23, Supporting Information). This clearly supports our interpretation that, first, electron transfer from the COF to the PCBM takes place, and second, that the interpenetrated system provides an appropriate interface for charge dissociation.

CONCLUSIONS

The novel benzodithiophene-based covalent organic framework, BDT-COF, was synthesized as a bulk crystalline mesoporous material, which exhibits high surface area and significant thermal stability. Oriented, thin crystalline porous films of BDT-COF were synthesized on different polycrystalline surfaces, in particular metal oxides substrates, such as ITO-coated glass and ITO-coated glass modified with NiO as hole-selective layer. Krypton sorption analysis demonstrates the mesoporosity of the thin BDT-COF film. The open hexagonal COF-channels perpendicular to the surface provide a perfect architecture for interpenetrated host−guest systems. Our observations suggest that the thin BDT films are formed through an island growth mode. The growth of thin BDT-COF films on a variety of surfaces also allows for studying their optical properties. Thin BDT-COF films exhibit two major optical absorbance bands in the UV spectral region. The thin oriented BDT-COF films served as a host for different fullerene-derived acceptor molecules, [60]PCBM and [70]PCBM. The photoluminescence of the BDT-COF film was quenched to a large extent by both acceptors, indicating that charge transfer occurred. We expect that our newly developed method of film growth will facilitate

the study of charge separation and collection and the effect of molecular packing on the transport behavior in ordered organic interpenetrated systems. Specifically, it will be of interest to further understand the impact of the mode of π-stacking in oriented thin COF films, the conjugation in the 2D-network, the COF wall thickness, and the type of donor−acceptor interactions to realize the potential of these intriguing ordered materials.

METHODS

Materials. *General.* All materials (if not noted otherwise) were purchased from Aldrich, Fluka or Acros in the common purities purum and puriss. 2,3,6,7,10,11-Hexahydroxytriphenylene (HHTP) was purchased from TCI Europe. [6,6]-Phenyl C_{61} butyric acid methyl ester ([60]PCBM) and [6,6]-phenyl C_{71} butyric acid methyl ester ([70]PCBM) were purchased from Solenne BV. All materials were used without further purification. The building block benzo[1,2-*b*:4,5-*b*′]dithiophene-2,6-diyldiboronic acid (BDTBA) was prepared as described below. Analytical data of intermediates were found to match literature data.[56] The COF materials were handled in air.

Synthesis. All reactions for the preparation of the benzo[1,2-*b*:4,5-*b*′]dithiophene-2,6-diyldiboronic acid (BDTBA) building block were carried out under an argon atmosphere in flame-dried glassware. Tetrahydrofuran (THF) was continuously refluxed and freshly distilled from sodium benzophenone ketyl under nitrogen. Yields refer to isolated yields of compounds estimated to be >95% pure as determined by NMR (25 °C) and capillary GC. NMR spectra were recorded as solutions in deuterated chloroform ($CDCl_3$) with residual chloroform (δ = 7.26 ppm for ^{1}H NMR and δ = 77.0 ppm for ^{13}C NMR), acetone-d_6 (δ = 2.05 ppm for ^{1}H NMR and δ = 206.3 ppm for ^{13}C NMR), respectively. Column chromatographic purification was performed using SiO_2 (0.040−0.063 mm, 230−400 mesh ASTM) from Merck.

Synthesis of 2,6-Di(trimethylsilyl)benzo[1,2-b:4,5-b′]dithiophene (1). In a flame-dried Schlenk flask, equipped with a magnetic stirring-bar, an argon inlet and a septum, benzo[1,2-*b*:4,5-*b*′]-dithiophene[56] (1.90 g, 10.0 mmol, 1 equiv) was dissolved in THF (50.0 mL, 0.2 M). The solution was cooled down to −30 °C and *n*-BuLi (4.93 mL, 11.0 mmol, 1.1 equiv, 2.23 M in hexane) was added dropwise. After the solution stirred for 30 min, chlorotrimethylsilane (TMS-Cl) (1.40 mL, 11.0 mmol, 1.1 equiv) was added and the solution was allowed to warm up to room temperature. After 45 min, the solution was again cooled to −30 °C, *n*-BuLi and TMS-Cl were added as described before, and the mixture was allowed to warm up to room temperature. The reaction was quenched with sat. aq $NaHCO_3$ (30 mL), extracted with diethyl ether (3 × 30 mL), dried over Na_2SO_4, and concentrated *in vacuo*. Purification by flash column chromatography (silica gel, isopentane isomer mixture) afforded **1** as a white solid (3.08 g, 92%). Mp: 189.2−190.9 °C. ^{1}H NMR (400 MHz, $CDCl_3$) δ/ppm = 8.29 (s, 2H), 7.49 (s, 2H), 0.42 (s, 18 H). ^{13}C NMR (100 MHz, $CDCl_3$) δ/ppm = 144.0, 141.1, 139.5, 130.2, 116.4, 0.04. IR (cm^{-1}): $\tilde{\nu}$ = 2953, 1739, 1506, 1439, 1367, 1246, 1170, 1059, 963, 866, 833, 752, 697. MS (70 eV, EI) *m*/*z* (%) = 336 (12), 335 (22), 334 (100) [M^+], 321 (13), 320 (19), 319 (71), 152 (24), 73 (30). HRMS for $C_{16}H_{22}S_2Si_2$ (334.0701): found 334.0685.

Benzo[1,2-b:4,5-b′]Dithiophene-2,6-diyldiboronic Acid (2). 2,6-Di(trimethylsilyl)benzo[1,2-*b*:4,5-*b*′]dithiophene (1.67 g, 5 mmol, 1 equiv) was dissolved in DCM (20 mL) at 0 °C. BBr_3 (1 mL, 10.5 mmol, 2.1 equiv) was added, and the reaction mixture was stirred for 12 h. The reaction was quenched by adding 1 M NaOH/ice mixture (40 mL), and the phases were separated. The aqueous phase was washed with DCM (2x 20 mL), then adjusted to pH 7 with 2 M HCl and extracted with ethyl acetate (3× 20 mL). The combined organic phases were dried over Na_2SO_4 and concentrated *in vacuo* to afford **2** as a white solid (0.95 g, 68%). Mp: 313.1−315.2 °C. ^{1}H NMR (300 MHz, $CDCl_3$) δ/ppm = 8.44 (s, 2H), 8.00 (s, 2H), 7.79 (s, 4H). ^{13}C NMR (75 MHz, $CDCl_3$) δ/ppm = 140.4, 139.6, 131.9, 117.0. IR (cm^{-1}): $\tilde{\nu}$ = 3351, 1541, 1435, 1398, 1366, 1341, 1312, 1177, 1163, 1106, 1033, 866, 645. HRMS (ESI) for $C_{10}H_8B_2O_4S_2$ (278.0050): found 276.9973 [M − H^+].

BDT-COF Synthesis. A conventional stainless steel autoclave equipped with a 3 mL Teflon liner was charged with BDTBA (**2**) (14.2 mg, 0.051 mmol) and HHTP (11.0 mg, 0.034 mmol). The reaction mixture was suspended in 1.5 mL of a 1:1 (v/v) solution of mesitylene/dioxane and heated for 72 h at 100 °C. The dark green precipitate was isolated by filtration and washed with dry acetone (3 mL).

BDT-COF Thin Film Synthesis. A conventional stainless steel autoclave equipped with a 20 mL Teflon liner was charged with BDTBA (**2**) (16.2 mg, 0.058 mmol) and HHTP (12.5 mg, 0.038 mmol). The reaction mixture was suspended in 5 mL of a 1:1 (v/v) solution of mesitylene/dioxane. Two clean ITO-coated glass substrates were placed horizontally on a homemade, ∏-shaped Teflon holder equipped with three slide compartments. The Teflon holder was placed into the starting material suspension in a way that the ITO surfaces face the bottom of the autoclave. The autoclave was then heated for 12 h at 100 °C. The substrates were then removed and washed with dry acetone (2 mL) and dried under a stream of N_2.

NiO-Coated Substrates. Indium tin oxide-coated glass slides (VisionTek, 12−15 Ω/sq) were cleaned by sonication in detergent solution, water, ethanol, and 2-propanol. A NiO precursor solution, consisting of 100 mM $Ni(OAc)_2 \cdot 4H_2O$ and 100 mM ethanolamine in HPLC-grade ethanol, was deposited *via* spin-coating and subsequently converted into a 10 nm thick NiO layer by heating to 300 °C for 45 min on a hot plate in air.

BDT-COF/Acceptor System. The thin BDT-COF films were activated at 150 °C for 2 h in high vacuum (10^{-5} mbar) and transferred to an argon-filled glovebox. The acceptor was infiltrated into the COF pores by spin-coating a 20 mg mL^{-1} solution of the fullerene acceptor in 1,2-dichlorobenzene.

X-ray diffraction analysis was carried out in reflection mode using a Bruker D8 Discover with Ni-filtered Cu Kα-radiation (1.5406 Å) and a position-sensitive detector (LynxEye). Small and wide angle X-ray scattering (SWAXS) was carried out with a SAXSess system (Anton Paar) equipped with an image plate. The sample was subjected to the X-ray beam at a grazing angle of 0.35° with respect to the primary beam. The X-rays scattered perpendicular *q*(*y*) and parallel *q*(*z*) to the surface normal were detected by an image plate covering wide angles, corresponding to 42° 2θ in the *q*(*z*) axis and 6° 2θ in *q*(*y*) axis. The wavelength of the incident beam was λ = 0.154 nm (Cu Kα); the sample−detector distance was 260.2 mm. Fourier-transform infrared spectra of samples were measured with a Bruker Equinox 55 equipped with a PIKE MIRacle ATR-unit at room temperature. Scanning electron microscope images were recorded with Jeol 6500F and Zeiss Ultra Plus field emission scanning electron microscopes. Transmission electron microscopy data were obtained with a FEI TITAN 80−300 microscope at an acceleration voltage of 80 kV. ^{11}B and ^{13}C MAS NMR spectra were recorded on a Bruker DSX Avance 500 with a magnetic field of 11.2 T. A 4 mm MAS triple-resonance sample head was used. The frequency of the rotors was 10 kHz. ^{11}B-NMR spectra were recorded with a single pulse program with 90 scans and a delay time of 1 s. For ^{13}C−CP-MAS NMR spectra, 1808 scans were performed with a delay time of 2 s. TG measurements were performed in a stream of synthetic air (25 mL/min) on a Netzsch STA 440 C TG/DSC. The measurements were carried out with a heating rate of 10 K/min and a temperature range from 30 to 900 °C. Nitrogen sorption isotherms were recorded on a Quantachrome Autosorb-1. Prior to the measurement of the adsorption isotherm, the sample was treated as follows. The product was washed with dry acetone, separated by filtration, and heated for 12 h at 150 °C under oil pump vacuum. The calculation of the pore size distribution was done using the NLDFT model with a carbon

kernel for cylindrical pores, using the desorption branch. Kr sorption experiments were carried out with an Autosorb iQ from Quantachrome Instruments at 77.3 K (liquid nitrogen temperature), assuming a saturation vapor pressure of p_0 = 217 Pa for Kr. Sample outgassing was performed in vacuum for 12 h at room temperature. For the BET surface area calculation, a saturation vapor pressure of the supercooled liquid (321 Pa at 77.3 K) and a molecular cross-sectional area of 0.205 nm^2 were assumed.[57,58] Molecular geometry optimization was performed with Accelrys MS Modeling 4.4 using the universal force field method. The final hexagonal unit cell was calculated with the geometric parameters from the optimized structure. For the simulation of the PXRD patterns the Reflex module was used (a software package implemented in MS Modeling 4.4). UV−vis spectra were recorded on a Perkin-Elmer Lambda 1050 spectrometer equipped with a 150 mm integrating sphere and a Varian Cary 5000 spectrometer. Diffuse reflectance spectra of powders were recorded using a Praying Mantis (Harrick) accessory. Thin films were measured in transmission geometry and corrected for reflection losses and losses at the edges of the substrate. Photoluminescence quenching experiments were performed using a Photon Technology International QuantaMaster spectrometer with an excitation wavelength of 365 nm. The samples were positioned at an angle of 45° with respect to the incident beam and illuminated through the fused silica substrate. PL was detected at 90° with respect to the excitation beam. Time-resolved transient absorption spectra were measured using a home-built pump−probe setup. The setup is based on a Ti:sapphire regenerative amplifier (RegA 9060, Coherent), emitting linearly polarized 60 fs pulses (fwhm) with a pulse energy of 6 μJ at a central wavelength of 800 nm and a repetition rate of 90 kHz. Frequency doubling of a part of the pulse energy in a nonlinear optical β-barium-borate (BBO) crystal provided pump pulses at a wavelength of 400 nm, which are suitable for exciting the investigated thin COF films. For probing, a linearly polarized supercontinuum white-light spectrum was generated by focusing a part of the fundamental laser light at 800 nm onto a sapphire plate having a thickness of 2 mm within an optical parametric amplifier setup (Coherent OPA-9450). Spectral filtering allowed measuring at each of the desired probe wavelengths of 650 and 1050 nm, which were achieved by using dielectric interference bandpass filters (Thorlabs). Said filters were placed in the optical path after the white-light probe was transmitted through the sample, in order to prevent deteriorations of the probe pulse shape before reaching the sample. For the purpose of detecting polarons in COFs and PCBM, bandpass filters with a transmission wavelength range of 650 ± 10 and 1050 ± 10 nm, respectively, were used. With the used setup, a temporal resolution of about 350 fs was achieved. For all measurements shown in this manuscript, the polarization of pump and probe were kept parallel with respect to each other. Detection of the transmitted probe pulses was done with a Si-photodiode (Thorlabs), and the resulting photocurrent was read out by two lock-in amplifiers (Stanford Research) referenced to the laser repetition rate (90 kHz) and the sum frequency (96 kHz) of the repetition rate and chopping frequency (6 kHz). The latter was obtained by mechanically chopping the pump pulses.

Conflict of Interest: The authors declare no competing financial interest.

Acknowledgment. The authors gratefully acknowledge funding from the NIM excellence cluster (DFG) and from the Bavarian SolTech research network. D.D.M. gratefully acknowledges a Minerva post-doctoral fellowship. The research leading to these results has received funding from the European Research Council under the European Union's Seventh Framework Programme (FP7/2007-2013) / ERC grant agreement no 321339.

Supporting Information Available: BDT-COF structure characterization, simulation of BDT-COF crystal structure, characterization of thin BDT-COF film on ITO/NiO and gold substrates and transient absorption measurements. This material is available free of charge *via* the Internet at http://pubs.acs.org.

REFERENCES AND NOTES

1. Côté, A. P.; Benin, A. I.; Ockwig, N. W.; O'Keeffe, M.; Matzger, A. J.; Yaghi, O. M. Porous, Crystalline, Covalent Organic Frameworks. *Science* **2005**, *310*, 1166–1170.
2. Côté, A. P.; El-Kaderi, H. M.; Furukawa, H.; Hunt, J. R.; Yaghi, O. M. Reticular Synthesis of Microporous and Mesoporous 2D Covalent Organic Frameworks. *J. Am. Chem. Soc.* **2007**, *129*, 12914–12915.
3. El-Kaderi, H. M.; Hunt, J. R.; Mendoza-Cortes, J. L.; Côté, A. P.; Taylor, R. E.; O'Keeffe, M.; Yaghi, O. M. Designed Synthesis of 3D Covalent Organic Frameworks. *Science* **2007**, *316*, 268–272.
4. Uribe-Romo, F. J.; Doonan, C. J.; Furukawa, H.; Oisaki, K.; Yaghi, O. M. Crystalline Covalent Organic Frameworks with Hydrazone Linkages. *J. Am. Chem. Soc.* **2011**, *133*, 11478–11481.
5. Colson, J. W.; Dichtel, W. R. Rationally Synthesized Two-Dimensional Polymers. *Nat. Chem.* **2013**, *5*, 453–465.
6. Ding, S.-Y.; Wang, W. Covalent Organic Frameworks (COFs). From Design to Applications. *Chem. Soc. Rev.* **2013**, *42*, 548–568.
7. Feng, X.; Ding, X. S.; Jiang, D. L. Covalent Organic Frameworks. *Chem. Soc. Rev.* **2012**, *41*, 6010–6022.
8. Furukawa, H.; Yaghi, O. M. Storage of Hydrogen, Methane, and Carbon Dioxide in Highly Porous Covalent Organic Frameworks for Clean Energy Applications. *J. Am. Chem. Soc.* **2009**, *131*, 8875–8883.
9. Han, S. S.; Furukawa, H.; Yaghi, O. M.; Goddard, W. A., III Covalent Organic Frameworks as Exceptional Hydrogen Storage Materials. *J. Am. Chem. Soc.* **2008**, *130*, 11580–11581.
10. Doonan, C. J.; Tranchemontagne, D. J.; Glover, T. G.; Hunt, J. R.; Yaghi, O. M. Exceptional Ammonia Aptake by a Covalent Organic Framework. *Nat. Chem.* **2010**, *2*, 235–238.
11. Ding, S. Y.; Gao, J.; Wang, Q.; Zhang, Y.; Song, W. G.; Su, C. Y.; Wang, W. Construction of Covalent Organic Framework for Catalysis: Pd/COF-LZU1 in Suzuki-Miyaura Coupling Reaction. *J. Am. Chem. Soc.* **2011**, *133*, 19816–19822.
12. Wan, S.; Guo, J.; Kim, J.; Ihee, H.; Jiang, D. A Belt-Shaped, Blue Luminescent, and Semiconducting Covalent Organic Framework. *Angew. Chem., Int. Ed.* **2008**, *47*, 8826–8830.
13. Wan, S.; Guo, J.; Kim, J.; Ihee, H.; Jiang, D. A Photoconductive Covalent Organic Framework: Self-Condensed Arene Cubes Composed of Eclipsed 2D Polypyrene Sheets for Photocurrent Generation. *Angew. Chem., Int. Ed.* **2009**, *48*, 5439–5442.
14. Spitler, E. L.; Dichtel, W. R. Lewis Acid-Catalysed Formation of Two-Dimensional Phthalocyanine Covalent Organic Frameworks. *Nat. Chem.* **2010**, *2*, 672–677.
15. Ding, X.; Chen, L.; Honsho, Y.; Feng, X.; Saenpawang, O.; Guo, J.; Saeki, A.; Seki, S.; Irle, S.; Nagase, S.; et al. An n-Channel Two-Dimensional Covalent Organic Framework. *J. Am. Chem. Soc.* **2011**, *133*, 14510–14513.
16. Ding, X.; Guo, J.; Feng, X.; Honsho, Y.; Guo, J.; Seki, S.; Maitarad, P.; Saeki, A.; Nagase, S.; Jiang, D. Synthesis of Metallophthalocyanine Covalent Organic Frameworks that Exhibit High Carrier Mobility and Photoconductivity. *Angew. Chem., Int. Ed.* **2011**, *50*, 1289–1293.
17. Feng, X.; Chen, L.; Dong, Y.; Jiang, D. Porphyrin-Based Two-Dimensional Covalent Organic Frameworks: Synchronized Synthetic Control of Macroscopic Structures and Pore Parameters. *Chem. Commun.* **2011**, *47*, 1979–1981.
18. Dogru, M.; Handloser, M.; Auras, F.; Kunz, T.; Medina, D.; Hartschuh, A.; Knochel, P.; Bein, T. A Photoconductive Thienothiophene-Based Covalent Organic Framework Showing Charge Transfer Towards Included Fullerene. *Angew. Chem., Int. Ed.* **2013**, *52*, 2920–2924.
19. Bertrand, G. H. V.; Michaelis, V. K.; Ong, T.-C.; Griffin, R. G.; Dinca, M. Thiophene-Based Covalent Organic Frameworks. *Proc. Natl. Acad. Sci. U.S.A.* **2013**, *110*, 4923–4928.
20. Chen, X.; Addicoat, M.; Irle, S.; Nagai, A.; Jiang, D. Control of Crystallinity and Porosity of Covalent Organic Frameworks by Managing Interlayer Interactions Based on

Self-Complementary pi-Electronic Force. *J. Am. Chem. Soc.* **2013**, *135*, 546–549.
21. Feng, X.; Chen, L.; Honsho, Y.; Saengsawang, O.; Liu, L. L.; Wang, L.; Saeki, A.; Irle, S.; Seki, S.; Dong, Y. P.; *et al.* An Ambipolar Conducting Covalent Organic Framework with Self-Sorted and Periodic Electron Donor-Acceptor Ordering. *Adv. Mater.* **2012**, *24*, 3026–3031.
22. Patwardhan, S.; Kocherzhenko, A. A.; Grozema, F. C.; Siebbeles, L. D. A. Delocalization and Mobility of Charge Carriers in Covalent Organic Frameworks. *J. Phys. Chem. C* **2011**, *115*, 11768–11772.
23. Wan, S.; Gandara, F.; Asano, A.; Furukawa, H.; Saeki, A.; Dey, S. K.; Liao, L.; Ambrogio, M. W.; Botros, Y. Y.; Duan, X.; *et al.* Covalent Organic Frameworks with High Charge Carrier Mobility. *Chem. Mater.* **2011**, *23*, 4094–4097.
24. Tang, C. W. 2-Layer Organic Photovoltaic Cell. *Appl. Phys. Lett.* **1986**, *48*, 183–185.
25. Peumans, P.; Uchida, S.; Forrest, S. R. Efficient Bulk Heterojunction Photovoltaic Cells Using Small-Molecular-Weight Organic Thin Films. *Nature* **2003**, *425*, 158–162.
26. Uhrich, C.; Schueppel, R.; Petrich, A.; Pfeiffer, M.; Leo, K.; Brier, E.; Kilickiran, P.; Baeuerle, P. Organic Thin-Film Photovoltaic Cells Based on Oligothiophenes with Reduced Bandgap. *Adv. Funct. Mater.* **2007**, *17*, 2991–2999.
27. Pettersson, L. A. A.; Roman, L. S.; Inganas, O. Modeling Photocurrent Action Spectra of Photovoltaic Devices Based on Organic Thin Films. *J. App. Phys.* **1999**, *86*, 487–496.
28. Sonar, P.; Singh, S. P.; Li, Y.; Ooi, Z.-E.; Ha, T.-j.; Wong, I.; Soh, M. S.; Dodabalapur, A. High Mobility Organic Thin Film Transistor and Efficient Photovoltaic Devices Using Versatile Donor-Acceptor Polymer Semiconductor by Molecular Design. *Energy Environ. Sci.* **2011**, *4*, 2288–2296.
29. Forrest, S. R. Ultrathin Organic Films Grown by Organic Molecular Beam Deposition and Related Techniques. *Chem. Rev.* **1997**, *97*, 1793–1896.
30. Guo, J. X. Y.; Jin, S.; Chen, L.; Kaji, T.; Honsho, Y.; Addicoat, M. A.; Kim, J.; Saeki, A.; Ihee, H.; Seki, S.; *et al.* Conjugated Organic Framework with Three-Dimensionally Ordered Stable Structure and Delocalized π Clouds. *Nat. Commun.* **2013**, *4*, 2736.
31. Moller, K.; Bein, T. Inclusion Chemistry in Periodic Mesoporous Hosts. *Chem. Mater.* **1998**, *10*, 2950–2963.
32. Wu, C. G.; Bein, T. Conducting Carbon Wires in Ordered, Nanometer-Size Channels. *Science* **1994**, *264*, 1013–1015.
33. Johnson, S. A.; Ollivier, P. J.; Mallouk, T. E. Ordered Mesoporous Polymers of Tunable Size from Colloidal Silica Templates. *Science* **1999**, *283*, 963–965.
34. Brezesinski, T.; Wang, J.; Tolbert, S. H.; Dunn, B. Ordered Mesoporous Alpha-MoO_3 with Iso-Oriented Nanocrystalline Walls for Thin-Film Pseudocapacitors. *Nat. Mater.* **2010**, *9*, 146–151.
35. Richman, E. K.; Brezesinski, T.; Tolbert, S. H. Vertically Oriented Hexagonal Mesoporous Films Formed Through Nanometre-Scale Epitaxy. *Nat. Mater.* **2008**, *7*, 712–717.
36. Brezesinski, T.; Groenewolt, M.; Pinna, N.; Amenitsch, H.; Antonietti, M.; Smarsly, B. M. Surfactant-Mediated Generation of Iso-Oriented Dense and Mesoporous Crystalline Metal-Oxide Layers. *Adv. Mater.* **2006**, *18*, 1827–1831.
37. Goux, A.; Etienne, M.; Aubert, E.; Lecomte, C.; Ghanbaja, J.; Walcarius, A. Oriented Mesoporous Silica Films Obtained by Electro-Assisted Self-Assembly (EASA). *Chem. Mater.* **2009**, *21*, 731–741.
38. Walcarius, A.; Sibottier, E.; Etienne, M.; Ghanbaja, J. Electrochemically Assisted Self-Assembly of Mesoporous Silica Thin Films. *Nat. Mater.* **2007**, *6*, 602–608.
39. Colson, J. W.; Woll, A. R.; Mukherjee, A.; Levendorf, M. P.; Spitler, E. L.; Shields, V. B.; Spencer, M. G.; Park, J.; Dichtel, W. R. Oriented 2D Covalent Organic Framework Thin Films on Single-Layer Graphene. *Science* **2011**, *332*, 228–231.
40. Spitler, E. L.; Colson, J. W.; Uribe-Romo, F. J.; Woll, A. R.; Giovino, M. R.; Saldivar, A.; Dichtel, W. R. Lattice Expansion of Highly Oriented 2D Phthalocyanine Covalent Organic Framework Films. *Angew. Chem., Int. Ed.* **2012**, *51*, 2623–2627.
41. Li, Y. F. Molecular Design of Photovoltaic Materials for Polymer Solar Cells: Toward Suitable Electronic Energy Levels and Broad Absorption. *Acc. Chem. Res.* **2012**, *45*, 723–733.
42. Huo, L. J.; Hou, J. H. Benzo 1,2-b:4,5-b′ dithiophene-Based Conjugated Polymers: Band Gap and Energy Level Control and Their Application in Polymer Solar Cells. *Polym. Chem.* **2011**, *2*, 2453–2461.
43. Liang, Y. Y.; Yu, L. P. A New Class of Semiconducting Polymers for Bulk Heterojunction Solar Cells with Exceptionally High Performance. *Acc. Chem. Res.* **2010**, *43*, 1227–1236.
44. Sista, P.; Biewer, M. C.; Stefan, M. C. Benzo 1,2-b:4,5-b′ Dithiophene Building Block for the Synthesis of Semiconducting Polymers. *Macromol. Rapid Commun.* **2012**, *33*, 9–20.
45. Hou, J.; Park, M.-H.; Zhang, S.; Yao, Y.; Chen, L.-M.; Li, J.-H.; Yang, Y. Bandgap and Molecular Energy Level Control of Conjugated Polymer Photovoltaic Materials Based on Benzo[1,2-*b*:4,5-*b*′]dithiophene. *Macromolecules* **2008**, *41*, 6012–6018.
46. Zhou, E. J.; Cong, J. Z.; Hashimoto, K.; Tajima, K. A Benzoselenadiazole-Based Low Band Gap Polymer: Synthesis and Photovoltaic Application. *Macromolecules* **2013**, *46*, 763–768.
47. Fortunato, E.; Ginley, D.; Hosono, H.; Paine, D. C. Transparent Conducting Oxides for Photovoltaics. *Mater. Res. Bull.* **2007**, *32*, 242–247.
48. Smilgies, D. M. Scherrer Grain-Size Analysis Adapted to Grazing-Incidence Scattering with Area Detectors. *J. Appl. Crystallogr.* **2009**, *42*, 1030–1034.
49. Bartels, O.; Zukal, A. Krypton Adsorption Technique for Assessment of Structural Properties of Mesoporous Silica and Titania Thin Films. *J. Mater. Sci.* **2005**, *40*, 2603–2605.
50. Manders, J. R.; Tsang, S.-W.; Hartel, M. J.; Lai, T.-H.; Chen, S.; Amb, C. M.; Reynolds, J. R.; So, F. Solution-Processed Nickel Oxide Hole Transport Layers in High Efficiency Polymer Photovoltaic Cells. *Adv. Funct. Mater.* **2013**, *23*, 2993–3001.
51. Hinterholzinger, F. M.; Wuttke, S.; Roy, P.; Preusse, T.; Schaate, A.; Behrens, P.; Godt, A.; Bein, T. Highly Oriented Surface-Growth and Covalent Dye Labeling of Mesoporous Metal-Organic Frameworks. *Dalton Trans.* **2012**, *41*, 3899–3901.
52. Tautz, R.; Da Como, E.; Limmer, T.; Feldmann, J.; Egelhaaf, H.-J.; von Hauff, E.; Lemaur, V.; Beljonne, D.; Yilmaz, S.; Dumsch, I.; *et al.* Structural Correlations in the Generation of Polaron Pairs in Low-Bandgap Polymers for Photovoltaics. *Nat. Commun.* **2012**, *3*, 970.
53. Tautz, R.; Da Como, E.; Wiebeler, C.; Soavi, G.; Dumsch, I.; Froehlich, N.; Grancini, G.; Allard, S.; Scherf, U.; Cerullo, G.; *et al.* Charge Photogeneration in Donor-Acceptor Conjugated Materials: Influence of Excess Excitation Energy and Chain Length. *J. Am. Chem. Soc.* **2013**, *135*, 4282–4290.
54. Wiebeler, C.; Tautz, R.; Feldmann, J.; von Hauff, E.; Da Como, E.; Schumacher, S. Spectral Signatures of Polarons in Conjugated Co-Polymers. *J. Phys. Chem. B* **2013**, *117*, 4454–4460.
55. Guo, J.; Ohkita, H.; Benten, H.; Ito, S. Charge Generation and Recombination Dynamics in Poly(3-hexylthiophene)/Fullerene Blend Films with Different Regioregularities and Morphologies. *J. Am. Chem. Soc.* **2010**, *132*, 6154–6164.
56. Kashiki, T.; Shinamura, S.; Kohara, M.; Miyazaki, E.; Takimiya, K.; Ikeda, M.; Kuwabara, H. One-Pot Synthesis of Benzo[*b*]thiophenes and Benzo[*b*]selenophenes from *o*-Halo-Substituted Ethynylbenzenes: Convenient Approach to Mono-, Bis-, and Tris-Chalcogenophene-Annulated Benzenes. *Org. Lett.* **2009**, *11*, 2473–2475.
57. McClella, A. L.; Harnsber, H. F. Cross-Sectional Areas of Molecules Adsorbed on Solids Surfaces. *J. Colloid Interface Sci.* **1967**, *23*, 577–599.
58. Lowell, S.; Shields, J. E; Thomas, M. A; Thommes, M. *Characterization of Porous Solids and Powders Surface Area, Pore Size and Density*; Scarlett, B., ed.; Springer: Dordrecht, 2006; pp 71−80.